Lasers in Manufacturing Conference 2021

Joining dissimilar materials: a new approach based on laser beam welding and melt displacement by electromagnetic forces

Jennifer Heßmann[a,*], Marcel Bachmann[a], Kai Hilgenberg[a]

[a]*Bundesanstalt für Materialforschung und -prüfung (BAM), Unter den Eichen 87, 12205 Berlin, Germany*

Abstract

In order to reduce weight of vehicles, the interest in multi-material-design has been growing within the last few years. For vehicles the combination of steel and aluminium alloys offers the most promising compromise between weight, strength and formability. Thermal joining of these dissimilar materials is still a challenge to overcome. A possible approach is a new joining technology, whereby a combination of laser beam welding and contactless induced electromagnetic forces are used to displace the generated melt of one joining partner into a notch of the other. This paper presents the working principle and shows numerical analyses to improve the understanding of this joining process. The simulations help to calculate the thermal development of the joining partners, which is important for the formation of intermetallic phases. Furthermore, the calculation of the time required for a complete displacement is possible. The numerical results are validated by experimental results.

Keywords: Electromagnetic forces; Lorentz forces; Laser beam welding; Joining technology; Dissimilar materials; Steel; Aluminium alloy

1. Introduction

Environmental requirements, such as the reduction of CO_2 emissions, increasing customer demands in comfort and the higher desired range of electric vehicles, force the automotive industry to reduce the weight of body structures. The multi-material-design has become of significant interest for new lightweight construction concepts in the last two decades (Kleemann et al., 2017). The weight is reduced by replacing heavier materials by lighter alternatives without negatively affecting the functional properties. In addition to weight reduction, this lightweight design concept offers the possibility of improved mechanical performance

* Corresponding author. Tel.: +49-30-8104-2756;
E-mail address: Jennifer.hessmann@bam.de

of the assemblies by using the specific material properties. Beside steel, aluminium is one of the most important construction materials. Furthermore, this material combination offers the best compromise between static strength and formability. The work by Gándara, 2012 presents that the advantageous combination of low weight, good strength and workability of aluminium resulted in an increased usage for automotive applications. This work also shows, that by using aluminium for the vehicle body structure, a total weight reduction of at least 30 % is possible without affecting the vehicle performance.

The combination of dissimilar materials creates new challenges for joining processes (Friedrich, 2017). Especially when it involves the joining of load-bearing components in the vehicle. The different physical properties of the materials, such as melting temperature, thermal conductivity and expansion coefficients have to be regarded. Another problem of thermal joining of steel and aluminium is the insolvability of the materials in each other, which leads to intermetallic phases. The work of Wang et al, 2016 shows that during laser beam welding, these brittle phases can reduce the quality of the weld and create areas of cracking. Conventional joining methods such as adhesive bonding require a complex surface preparation of the components. Furthermore, the work pieces have to be fixed until the adhesives have hardened and cannot be further processed directly. Mechanical joining processes such as riveting or the combination with thermal joining processes such as resistance element welding require auxiliary joining elements, which have a negative influence on the lightweight construction balance. To increase the application possibilities of multi-material design, it is essential to improve joining technologies. For a better lightweight construction balance, it is advantageous to develop a thermal joining technology that does not require any auxiliary elements or filler materials and melts only one joining partner.

This new approach is based on the combination of laser beam welding and contactless induced electromagnetic forces to displace the generated melt of one joining partner in a controlled way into a notch of the second joining partner, to create material- and form-fitting joints for overlap configurations. The additional form-fit will improve the strength of the weld. For this joining technology no filler materials or auxiliary joining elements are necessary, and it can be used for spot shaped or line shaped joints. The single process steps are illustrated in Figure 1.

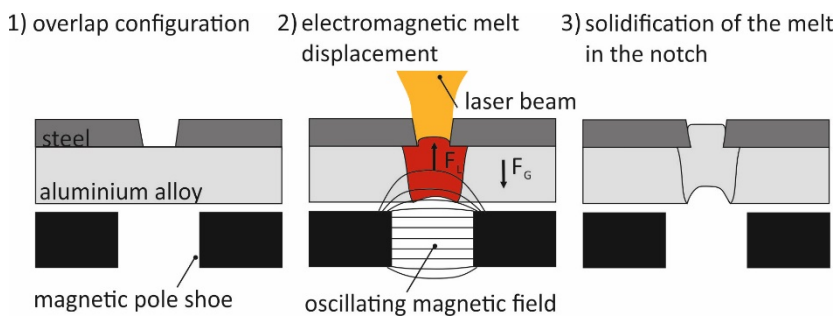

Fig. 1. Process steps of the new joining technology

The overlap configuration consists of two joining partners, whereby the upper joining partner must have the higher melt temperature and a notch. The laser beam melts the lower joining partner trough the notch of the upper joining partner to create a defined melt pool. The melting of the upper joining partner has to be avoided. An oscillating magnetic field is placed below the overlap configuration, which induces contactless electromagnetic forces (F_L) directed against the gravity force (F_g) into the lower joining partner. This working principle was already introduced in the studies of Avilov et al., 2012, Avilov et al., 2016 and Bachmann et al.,

2012, Bachmann et al., 2014 as weld pool support. Here, these electromagnetic forces displace the generated melt pool upwards into the notch of the upper joining partner. The laser beam is shut down after the completed displacement of the melt and a material- and form-fitting joint is created.

In this study a numerical analysis was carried out to improve the understanding of this joining technology, especially to predict the required time for the whole displacement process and the development of the temperature of the joining partners. The numerical analysis is validated by experiments. The investigation of the intermetallic phases is carried out by electro-microscopy and micro hardness tests.

2. Experimental setup and numerical analysis

For the experiments a self-constructed magnet system was placed below an overlap configuration of 1 mm steel sheet and 2 mm aluminium alloy sheet. The notch of the steel sheet had a diameter of 1.6 mm. The range of the oscillating magnetic field was limited to the thickness of the aluminium sheet according to the skin effect. Therefore, the magnetic system was used at a frequency of 3750 Hz. This limitation is important to minimize the influence of the ferromagnetic steel on the induced electric currents. The magnetic system was calibrated at room temperature by hall sensor measurements between the magnetic pole shoes. The details of the self-constructed magnetic system can be read in the work of Heßmann et al., 2020. A solid-state laser (IPG, 20 kW ytterbium fiber laser) was used to melt the lower joining partner trough the notch of the upper joining partner. The laser beam was focused on the surface of the lower joining partner and not tilted. Argon with 20 l min^{-1} was used as shielding gas. For the lower joining partner an EN AW 5754 aluminium wrought alloy was used, and the upper joining partner was 1.0330 steel. The surfaces of the sheets were cleaned by ethanol and fixed in a self-constructed sample holder to minimize the gap between the sheets. The parameters of the laser process were chosen by pretests for generation of reproducibly shaped melt pools without process pores and less melt pool ejections. The magnetic flux density was varied in five steps within this study and measured by a hall sensor placed between the magnetic pole shoes. Each parameter set was repeated four times and between the single spot joints a waiting time was used to ensure a similar thermal starting situation. So, a total number of 30 joints were produced. The experimental parameters are listed in Table 1.

Table 1. The optical components and used experimental process parameters

parameter	value	unit
wavelength	1070	nm
laser fiber diameter	200	µm
beam parameter product	11	mm × mrad
focal length	350	mm
used laser power	2.5	kW
beam duration	200	ms
magnetic flux density	0–196	mT
frequency	3750	Hz

The experiments were monitored by a high-speed camera (Fastcam, type SA4) and three thermocouples (type K) on the surface of the steel sheet per spot joint. The thermocouples were manually fixed close to the edge of the notch of the steel sheet to measure the thermal load on the upper joining partner. The exact location of the placed thermocouples was measured by stereo microscopy. The analysis of microstructure and the intermetallic phases were carried out on cross sections (etching: 2 % Nital and 2 % NaOH) by using microscopy, scanning electron microscopy (Thermo Fisher, type Phenom XL) and micro hardness tests (Vickers HV 0.1). A total number of five profile hardness measurements were carried out for each parameter set.

The process monitoring of the whole temperature development of both joining partners is very complex and difficult. Especially the measurement of temperatures at the melt pool boundary below the surface is not possible. So numerical analysis was used in addition to the experimental tests. For the numerical study, the software Comsol Multiphysics was used to create an overlap configuration of 1 mm steel sheet (1.0034) and 2 mm aluminium sheet (EN AW-6181). The temperature dependent material properties are close to the material used in the experiment and taken from literature and listed in Table 2. The steel sheet had the same notch of 1.6 mm as the joints in the experiments.

Table 2. The used material properties of steel (MatWeb, 2020 and Verein Deutscher Ingenieure, 2013) and aluminium (Schwenk, 2007 and Mills, 2002) at melt temperature

material properties	symbol	steel (1.0034)	aluminium (EN AW-6181)	unit
melting range	$T_m \pm \delta T$	1699	911 ± 18.5	K
evaporation temperature	T_{evap}	3135	2720	K
mass density	ρ	7850	2450	kg m^{-3}
heat capacity	c_p	846	1165	J kg^{-1} K^{-1}
thermal conductivity	λ	27.3	100	W m^{-1} K^{-1}
dynamic viscosity	η	–	1.1×10^{-3}	Pa s
surface tension	Υ	–	0.871	N m^{-1}
electrical resistivity	$\rho_{el} = \sigma^{-1}$	1.22×10^{-6}	24.77×10^{-8}	Ω m

To reduce the complexity of the model and the calculation time of the numerical study two independent models were prepared. A 3D electromagnetic model was used to analyse the spatial distribution of the five-step varied induced electromagnetic forces in the melt pool of the lower joining partner. The detailed results are shown in the work of Heßmann et al., 2020. The electromagnetic force distribution in horizontal x- and y-directions of the melt pool within the notch differs less than 10 %, so it can be transferred to an averaged 2D distribution.

The second model was a 2D transient thermo-fluid dynamic model to calculate the generation of the melt and the process of melt displacement to indicate the required time and the thermal development of the joining partners. The overlap configuration of the joining partners was created in the same way as in the 3D model. In this model the heat transfer between the metal sheets and air also the fluid dynamic of the aluminium melt pool by induced magnetic forces were considered. For the transition between the liquid aluminium alloy and the air, the phase field method was used. The flow in the air has no influence of the results of the study, so the air was modelled with simplifications as a laminar incompressible fluid like in the

study of Bruyere et al., 2013. For deep penetration welding a volume heat source was used as presented in the work of Lu et al., 2015. This heat source was modified to a 2D rotationally symmetrical heat source. The input values of the heat source were 2.5 kW for the laser power and 200 ms laser-on time like in the experiments. The Navier-Stokes equations for laminar and incompressible flows were solved. The five different induced Lorentz forces (0 mT – 196 mT at 3750 Hz) were taken as a calculated force distribution from the 3D model and simplified to an averaged 2D force distribution as described and applied to the aluminium melt pool of the second model. Other flows and forces like Marangoni convection, free convection, vapor friction, and recoil forces of the keyhole were not considered. Further details of the numerical analysis can be found in the work of Heßmann et al., 2020. The 2D model is schematically shown in Figure 2.

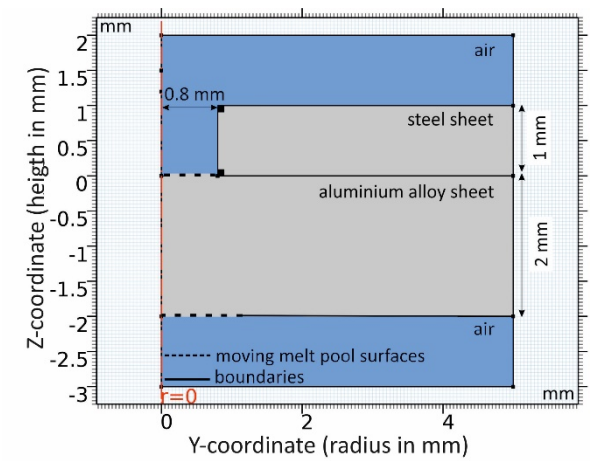

Fig. 2. The 2D model for numerical analysis

The prepared cross sections of the experimental joints were used for comparison of the calculated melt contours of the aluminium alloy and the heat affected zone (HAZ) of the steel sheet. The thermocouple measurements on the steel sheet were used to validate the numerical temperature distribution of the top of the upper joining partner.

3. Results and Discussion

The numerical results show that the effective range of magnetic flux density is 117 mT – 196 mT for a complete melt displacement in short process times below 200 ms. The required time for melt displacement and the thermal development of the joining partners is shown in Figure 3. With higher magnetic flux density, the displacement needs less time compared to lower magnetic flux densities. At 117 mT the displacement needs 165 ms and the aluminium melt is heated to 1000 K at the melt pool edge and to 2000 K in the center. When the aluminium melt moves upwards, the changed heat conduction in the steel layer results in a heat accumulation in the aluminium melt. The changed heat flow also results in an increasing width of the aluminium melt pool directly below the steel sheet. The steel has a HAZ with a maximum temperature of approximately 1200 K. By increasing the magnetic flux density to 196 mT, the displacement process can be shortened to 100 ms. Furthermore, the width of the HAZ (> 1000 K) of the steel sheet can be reduced from 450 µm to 260 µm. In the case of the higher magnetic flux density of 196 mT the melt pool is smaller

compared to the lower magnetic flux densities. The short total process time and the lower heat input results in a smaller melt pool.

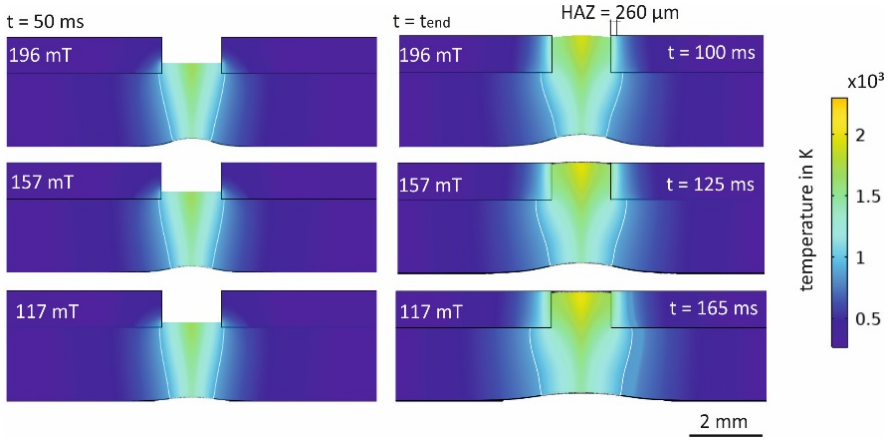

Fig. 3. Calculated temperature distribution of the joining partners and required time for the completed displacement process

The calculated contours of the melt pool, the prediction of the temperature of the steel sheet and the HAZ fits well to the experimental results considering the simplification of the numerical model. The comparison of numerical and experimental results is exemplary shown for 196 mT, 3750 Hz, 2.5 kW, 100 ms in Figure 4.

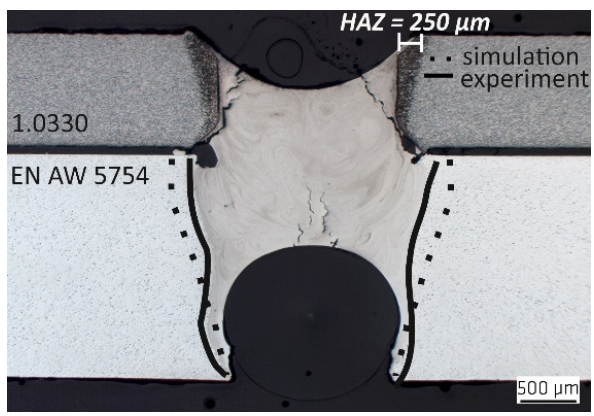

Fig. 4. Exemplary validation of numerical results with experimental results at a magnetic flux density of 196 mT, frequency of 3750 Hz, laser power of 2.5 kW and laser duration of 100 ms

The experimental results confirm the numerical prediction of the required process time for a completed melt displacement, for example 100 ms at 196 mT. Furthermore, the experimental results confirm the numerical results that magnetic flux densities of 117 mT – 196 mT are necessary for a complete melt pool displacement within 200 ms. The aluminium melt pool surface sinks down by the collapse of the keyhole after the laser is turned off. The aluminium melt has to fill the hole of the collapsed keyhole. The numerical and experimental measurements of the temperature of the steel sheet are shown in Table 3.

Table 3. Comparison of the numerical and experimental results of the temperature of the steel sheet at the end of each process time

magnetic flux density in mT	process time in ms	numerical temperature in K	experimental temperature in K
117	165	1266	1206
157	125	1262	1196
196	100	1076	1134

Considering the measuring accuracy of the thermocouples, the simulated and experimental steel temperature at the end of process time fits well. During the displacement melt pool dynamics were observed by high-speed camera. The frequent collapsing and explosive opening of the keyhole results in a pulse-like vertical movement of the aluminium melt. This melt pool dynamics are already known for aluminium alloys at deep penetration welding and are described in the work of Okon et al., 2002. It results in a fluctuated contact of the melt and the steel sheet, which cause a non-uniform heating of the steel sheet and formation of the intermetallic phases. The formation of the intermetallic phases is exemplary shown for a magnetic flux density of 196 mT, frequency of 3750 Hz, laser power of 2.5 kW and laser duration of 100 ms in Figure 5 a.). The analysis by scanning electron microscope shows an intermetallic phase seam at the interface of steel and aluminium alloy with an average width of about 7 µm. This width is lower than the known critical value of 10 µm for laser beam joining described in the work of Radscheit, 1996. Next to this seam further needle-shaped phases grow in the aluminium melt up to the melt pool center. The exemplary averaged profile hardness measurement for 196 mT can be seen in Figure 5 b.). The aluminium is hardened by the formed intermetallic phases from 60 HV 0.1 to 110 HV 0.1 – 130 HV 0.1. At the interface between steel and aluminium, the hardness increases to 200 HV 0.1 – 250 HV 0.1. The formation of these phases and the corresponding hardness values are similar for all samples. No significant differences in intermetallic phase thickness occur in the short process times below 200 ms.

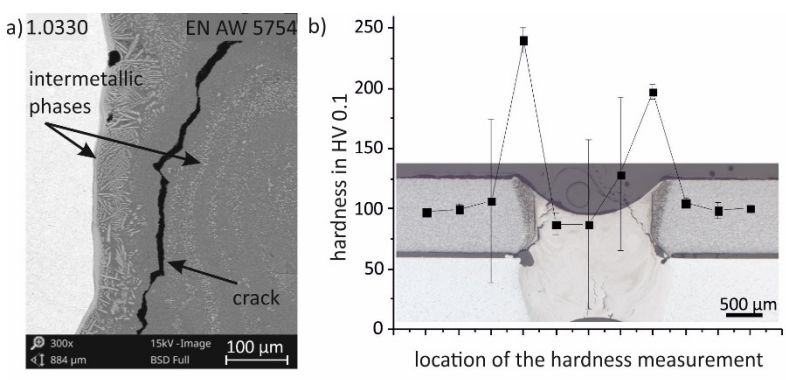

Fig. 5. a) Formation of intermetallic phases at magnetic flux density of 196 mT, frequency of 3750 Hz, laser power of 2.5 kW, laser duration of 100 ms and b) averaged profile hardness measurement

Detailed images of the intermetallic phases can be seen in Figure 6. Chemical analysis by scanning electron microscopy (EDX) shows that the intermetallic phase seam consists of 75 at.-% aluminium and 25 at.-% iron. The needle-shaped intermetallic phases of the aluminium melt pool contain 85 at.-% aluminium and 15 at.-%

iron. Cracks occurred in all displacement tests and were located along the intermetallic phase seams. This is probably caused by the different thermal expansion coefficients of the joined partners. Compared to steel, aluminium has a significant higher expansion coefficient. The strong shrinkage, that takes place during the solidification of the aluminium melt leads to crack formation at the intermetallic phase seam. Additionally, to the strains applied to the material, this area is brittle and thus exhibits a reduced ductility. In further investigations, this shrinkage might be compensated by creating a conical notch in order to reduce the formation of cracks. The conical shaped notch should positively support the direction of force of the shrinkage compared to straight hole edges for the formation of the joint so that the joining partners will be pulled into each other.

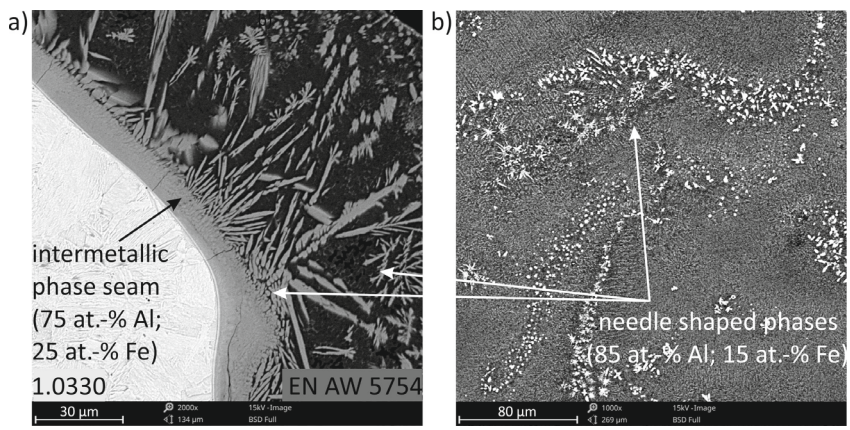

Fig. 6. Details of different intermetallic phases at a magnetic flux density of 196 mT, frequency of 3750 Hz, laser power of 2.5 kW and laser duration of 100 ms a) at the interface between steel and aluminium and b) in the center of the aluminium melt pool

4. Summary

This work shows that it is possible to create a joint between steel and aluminium with the presented approach of a new joining technology. The numerical process analysis improves the understanding of the joining technology. The numerical analysis supports the calculation of the required process time for a complete melt pool displacement. Using higher magnetic flux densities for example of approx. 196 mT, the displacement process is completed at 100 ms, so the laser beam can be shut down earlier compared to the chosen laser duration of 200 ms. This results in a reduced heating of the aluminium melt pool and a smaller heat affected zone of the steel sheet. In comparison, lower magnetic flux densities require more time for a complete melt displacement. Furthermore, the calculated temperature development of the joining partners helps to understand the formation of the intermetallic phases. The validation of the numerical process simulation by cross sections and thermocouple measurements resulted in a good agreement for the melt pool contours, the heat affected zone and the temperature distribution in the steel.

Acknowledgements

This research was funded by the Deutsche Forschungsgemeinschaft (DFG, German Research Foundation), grant number HI 1919/2-1; 646941. Financial funding is gratefully acknowledged.

References

Avilov, V., Fritzsche, A., Bachmann, M., Gumenyuk, A., Rethmeier, M., 2016. Full penetration laser beam welding of thick duplex steel plates with electromagnetic weld pool support, Journal of laser applications, Volume 28, Number 2, pp. 1-8, https://doi.org/10.2351/1.4944103

Avilov, V., Gumenyuk, A., Lammers, M., Rethmeier, M., 2012. PA position full penetration high power laser beam welding of up to 30 mm thick AlMg3 plates using electromagnetic weld pool support, Science and Technology of Welding and Joining, 17:2, pp. 128-133, https://doi.org/10.1179/1362171811Y.0000000085

Bachmann, M., Avilov, V., Gumenyuk, A., Rethmeier, M., 2012. Numerical simulation of full-penetration laser beam welding of thick aluminium plates with inductive support, Journal of Physics D: Applied Physics, 45, 035201, pp. 1- 13, stacks.iop.org/JPhysD/45/035201

Bachmann, M., Avilov, V., Gumenyuk, A., Rethmeier, M., 2014. Experimental and numerical investigation of an electromagnetic weld pool control for laser beam welding, Physics Procedia, 56, pp. 515-524, https://doi.org/10.1016/j.phpro.2014.08.006

Bruyere, V., Touvrey, C., Namy, P., 2013. Comparison between Phase Field and ALE Methods to model the Keyhole Digging during Spot Laser Welding, In Proceedings of the 2013 COMSOL Conference, Rotterdam, The Netherlands, 23–25, pp. 1–7

Friedrich, H., E., 2017. Leichtbau in der Fahrzeugtechnik, Springer. Vieweg. Wiesbaden. Germany. pp.628-667. DOI 10.1007/978-3-658-12295-9

Gándara, M., J., F., 2012. Aluminium: The metal of choice. Materials and Technology. 47/3, pp. 261-265, UDK 669.71:669.715

Heßmann, J., Bachmann, M., Hilgenberg, K., 2020. Numerical and experimental investigation of controlled weld pool displacement by electromagnetic forces for joining dissimilar materials, Journal Metals, MDPI, 10, 11, pp. 1447-1463, https://doi.org/10.3390/met10111447

Kleemann, S., Inkermann, D., Bader, B., Türck, E., Vietor, T., 2017. A Semi-formal approach to structure and access knowledge for multi-material-design, 21ST International conference on engineering design, ICED17. pp. 289-298, http://publikationsserver.tu-braunschweig.de/get/65110

Lu, F., Li, X., Tang, X., Cui, H., 2015. Formation and influence mechanism of keyhole-induced porosity in deep-penetration laser welding based on 3D transient modeling, International Journal of heat and mass Transfer, 90, pp. 1143-1152, doi:10.1016/j.ijheatmasstransfer.2015.07.041

MatWeb, 2020. Overview of materials for 6000 Series Aluminium Alloy. Available online: http://www.matweb.com/ (accessed on 22 July 2020).

Mills, K.C., 2002. Recommended Values of Thermophysical Properties for Selected Commercial Alloys; Woodhead Publishing Ltd: Cambridge, UK, pp. 9–71, 127–135.

Okon, P., Dearden, G., Watkins, K., Sharp, M., French, P., 2002. Laser Welding of Aluminium Alloy 5083, Journal of Laser Applications, pp. 1-11, https://doi.org/10.2351/1.5065620

Radscheit, C., 1996. Laserstrahlfügen von Aluminium mit Stahl, Dissertation Universität Bremen, Bremen: Verlag BIAS, pp. 1-108

Schwenk, C, 2007. FE-Simulation des Schweißverzugs laserstrahlgeschweißter dünner Bleche. Ph.D. Thesis, Degree-Granting Technical University, Berlin, Germany, pp. 47-57

Verein Deutscher Ingenieure, 2013. In VDI-Wärmeatlas, 11th ed.; VDI e.V.: Düsseldorf, Germany, pp. 3–1737.

Wang, P., Chen, X., Pan, Q., Madigan, B., Long, J., 2016. Laser welding dissimilar materials of aluminum to steel: an overview, The International Journal of Advanced Manufacturing Technology, 87, pp. 3081-3090, doi:10.1007/s00170-016-8725-y